



Published in final edited form as:

Cell Death Differ. 2011 April ; 18(4): 602–618. doi:10.1038/cdd.2010.117.

Short-chain fatty acids induced autophagy serves as an adaptive strategy for retarding mitochondria-mediated apoptotic cell death

Yong TANG^{a,b}, Yakun CHEN^a, Hongmei JIANG^{a,b}, Yin-Yuan Mo^a, and Daotai NIE^a

^aDepartment of Medical Microbiology, Immunology, and Cell Biology, Southern Illinois University School of Medicine and Simmons Cancer Institute, Springfield, IL 62794

^bMolecular Biology, Microbiology, and Biochemistry Graduate Program, Southern Illinois University Graduate School, Carbondale, IL 62901

Abstract

Short-chain fatty acids are the major by-products of bacterial fermentation of undigested dietary fibers in human large intestine. SCFAs, mostly propionate and butyrate, inhibit proliferation and induce apoptosis in colon cancer cells, but clinical trials had mixed results regarding the anti-tumor activities of SCFAs. Herein we demonstrate that propionate and butyrate induced autophagy in human colon cancer cells to dampen apoptosis whereas inhibition of autophagy potentiated SCFA induced apoptosis. Colon cancer cells, after propionate treatment, exhibited extensive characteristics of autophagic proteolysis: increased LC3-I to LC3-II conversion, acidic vesicular organelle development and reduced p62/SQSTM1 expression. Propionate-induced autophagy was associated with decreased mTOR activity and enhanced AMP kinase activity. The elevated AMPK α phosphorylation was associated with cellular ATP depletion and overproduction of reactive oxygen species due to mitochondrial dysfunction involving the induction of MPT and loss of ψ . In this context, mitochondria biogenesis was initiated to recover cellular energy homeostasis. Importantly, when autophagy was prevented either pharmacologically (3-MA or chloroquine) or genetically (knockdown of *ATG5* or *ATG7*), the colon cancer cells became sensitized toward propionate induced apoptosis through activation of caspase 7 and its downstream effector caspase-3. The observations indicate that propionate-triggered autophagy serves as an adaptive strategy for retarding mitochondria-mediated apoptotic cell death, whereas application of an autophagy inhibitor (Chloroquine) is expected to enhance the therapeutic efficacy of SCFAs in inducing colon tumor cell apoptosis.

Keywords

Short-chain fatty acids; autophagy; apoptosis; mitochondrial; colon cancer

Users may view, print, copy, download and text and data- mine the content in such documents, for the purposes of academic research, subject always to the full Conditions of use: http://www.nature.com/authors/editorial_policies/license.html#terms

Correspondence and Reprint Requests: Dr. Daotai Nie, Department of Medical Microbiology and Immunology, Southern Illinois University School of Medicine, PO Box 19626, Springfield, IL 62794. dnie@siu.edu. Fax: 217-545-3227..

Introduction

Colorectal cancer is the third most common cancer in the United States.¹ Cancer preventive constituents in the diet hold great promises as chemopreventive agents to reduce the incidence of cancer. Short-chain fatty acids (SCFA) are the major by-products of the bacterial fermentation and metabolism of undigested dietary fibers, particularly from degradation-resistant starches and dietary fiber in the human large intestine.² The molar ratio among the three major SCFAs (which constitute approximately 90% of the SCFAs generated in the lumen) varies according to a spectrum of factors, but the overall ratio is ~60:25:15 for acetate (2C): propionate (3C): butyrate (4C).³ Short-chain fatty acids, including but not limited to butyrate and propionate, are reported as antitumor agents which selectively induce differentiation, growth arrest, and apoptosis in colon cancer cells.^{4,5} The effect of SCFAs toward colon cancer prevention is also supported by epidemiological studies indicating that a diet high in fiber is associated with a decreased incidence and growth of colon cancers.⁶

Autophagy is an evolutionarily conserved catabolic process in which the cytoplasmic contents and organelles are transferred into double membrane vesicles, called “autophagosomes”.⁷ Autophagosome ultimately fuses with a lysosome, where its contents are broken down by degradative enzymes and subsequently recycled.⁸ Consequently, autophagy is a constitutive process responsible for the turnover of intracellular long-lived proteins and damaged organelles in maintaining cellular homeostasis. In addition, autophagy is highly regulated in tissue development, differentiation and remodeling.⁹ Autophagy is also implicated a spectrum of diseases such as tumor development, but its precise role is ambiguous.

A number of clinically available antineoplastic therapies, including radiotherapy and DNA-damaging chemotherapy, have been observed to induce autophagy in established human cancer cell lines and animal models.¹⁰⁻¹³ Whether autophagy induced by antineoplastic therapies facilitates tumor cell death or represents a self-defense mechanism for resisting therapy-mediated cell death remains controversial. Several observations support the argument that autophagy is detrimental to cancer cell survival, including the fact that the ability of radiation or chemotherapy to induce cell death in cancer cell lines that display resistance to apoptosis depends on autophagy induction.^{11,14} On the other hand, mounting evidence suggests that autophagy represents a self-protective strategy as autophagy guards cancer cells against antineoplastic treatment by abrogating the apoptotic cell death.^{15,16} These seemingly contradictory findings indicate that there is not a unique paradigm addressing the role of autophagy in tumorigenesis. Accordingly, it is conceivable that autophagy may have different roles in the different stages, or contexts, of tumorigenesis.

Evidence to date indicates that the antitumor effect of SCFAs is based on their ability to induce apoptotic cell death (Type I Programmed cell death (PCD)) in colon cancer cells.⁴ Interestingly, SCFAs have been reported to increase the expression of a broad range of mitochondria-related genes (177) and a spectrum of genes related to protein turnover (113), but the physiological relevance is yet to be understood.¹⁷ The goals of this study were to assess whether SCFAs, particularly propionate, induces another type of cell death--

autophagy and to study the importance of autophagy in the therapeutic efficacy of SCFAs toward colon cancer.

Materials and Methods

Materials

Human colon carcinoma cell lines HCT116 and SW480 were purchased from American Type Culture Collection. The 239T and phoenix™ Ampho packaging cell line were from Orbigen. HCT116 p53^{-/-} cell line, in which p53 is knockout by homologous recombination, was kindly gifted by Dr. Bert Vogelstein from the Johns Hopkins University, Baltimore, MD. Fetal bovine serum (FBS) was purchased from Invitrogen. Phospho-p70S6 Kinase (Thr421/Ser424) and total Akt were purchased from New England Biolabs. Purified mouse anti-PI3-Kinase was purchased from BD Transduction Laboratories. AMPK beta 1 Phospho (pS181) and AMPK gamma-1 (C-term) rabbit monoclonal antibody were purchased from Epitomics Inc. LC3 rabbit polyclonal antibody was kindly given by Dr. Jayanta Debnath. p62/SQSTM1, ATG7 and LAMP-2 antibody were purchased from Santa Cruz Biotechnology, Inc. Total OXPHOS human antibody cocktail (MS601) and MitoProfile® total OXPHOS+PDH ICC antibody kit (MS602) were purchased from MitoSciences Inc. Beta-actin was purchased from Sigma-Aldrich. All other antibodies were purchased from Cell Signaling Technology, Inc. Sodium propionate, sodium butyrate, Monodansylcadaverine (MDC), Chloroquine, N-acetylcysteine (NAC), Compound C and 3-Methyladenine (3-MA) were purchased from sigma. The regular PCR reagents and MTS solution were from Promega. DNAfectin™ liposome transfection reagent was purchased from Applied Biological Materials. Microtubule associated protein light chain 3 (GFP-LC3) retrovirus expression construct, was kindly given by Dr. Jayanta Debnath from the University of California.¹⁸ Four HuSH 29mer shRNA constructs against human *ATG5* (Locus ID = 9474), with sequences listed in table 1, were purchased from OriGene Technologies, Inc. Four pGIPZ lentiviral shRNA constructs against human *ATG7* and four pTRIPZ lentiviral shRNA constructs against human AMP, alpha 1 catalytic subunit (PRKAA1) were purchased from Open Biosystems. LysoTracker® Red DND-99, MitoTracker Deep Red FM, MitoTracker Green FM, Reactive Oxygen Species (ROS) Detection Reagent (carboxy-H₂DCFDA), Vybrant® Apoptosis Assay Kit (V35116) with Alexa Fluor® 488 annexin V, MitoTracker® Red dye, and MitoProbe™ Transition Pore Assay Kit (M34153) were purchased from Invitrogen.

Cell culture and transfection

HCT116 cells were grown in a RPMI 1640 medium supplemented with 10% FBS and Antibiotics-Antimycotics (100 units/ml penicillin, 100 µg/ml streptomycin and 250 µg/ml amphotericin B) in a humidified incubator under an atmosphere containing 5% CO₂ at 37 °C. Phoenix™ Ampho cells were grown in DMEM medium with 10% FBS and Antibiotics-Antimycotics. All cell lines were tested negative for mycoplasma contamination. MAP1LC3 (LC3), one of the mammalian homologues of yeast *ATG8*, is a well-established marker of autophagosome formation.¹⁹ In this study, we used a retroviral vector (pBABE) to generate cell lines stably expressing GFP-LC3.¹⁸ For this viral infection, approximately 10 million Phoenix™ Ampho cells were transfected with the plasmid by using DNAfectin™ liposome

transfection reagent. Viral supernatants were collected 48 hours after transfection, diluted 1:1 in fresh medium in the presence of polybrene (4 μ g/ml) and added to HCT116 and SW480 cells seeded in six-well plates at 30% confluence. After 24 h at 37 °C, the viral supernatant was replaced with a fresh aliquot. Three sequential rounds of infection were performed for each condition, after which more than 90% of the cells expressed the exogenous proteins. Generation of HCT116 and SW480 cells with *ATG5* knockdown by shRNA was performed according to the protocol described above. Regarding to *ATG7* pGIPZ lentiviral shRNA and *AMPK α* pTRIPZ lentiviral shRNA generations, 293T cells were transfected with *ATG7* shRNA or *AMPK α* constructs in the presence of pPACK packaging plasmid mist (Open Biosystems). The virus collection and target cells infection follow the same protocol above. HCT116 cells with *ATG7* pGIPZ lentiviral shRNA expression are marked by TurboGFP. HCT116 cells with *AMPK α* pTRIPZ lentiviral shRNA expression are marked by TurboRFP and regulated by a Tet-On® or Tet-Off® system.

Western blotting

HCT116 and SW480 cells subjected to different treatments were collected with ice-cold RIPA Buffer (Sigma, R0278) in the presence of a protease inhibitor cocktail (Sigma, S8830). Fifty micrograms of protein were fractionated by SDS-PAGE gels in a Bio-Rad Protean II system. After transferring proteins to a PVDF membrane, the membrane was blocked with Odyssey Blocking Buffer from LI-COR Biosciences for 60 min at room temperature and incubated with the primary antibody at appropriate dilutions in Odyssey Blocking Buffer at 4 °C overnight. After overnight incubation with appropriate primary antibodies, the membrane was washed (3 \times) with TBS-T for a total of 15 min, probed with fluorescently-labeled secondary antibody (1:5000) for 80 min at room temperature and washed (3 \times) with TBS-T for a total of 15 min. The immunoblots were visualized by an Odyssey Infrared Imaging System (LI-COR Biosciences).

Labeling of acidic compartments with LysoTracker and MDC

LysoTracker® Red DND-99 has been widely used as a probe to indicate autophagic activity in a variety of organisms.^{20,21} In brief, acidic vesicular organelles (AVO) were labeled with the dye (50 nM, Molecular Probes) diluted in prewarmed (37°C) RPMI 1640 medium for 15 min at 37. After incubation, the cells were rinsed once with serum-free medium and immediately observed with a BX41 fluorescence microscope (Olympus, Center Valley, PA). 20,000 cells per sample were determined by flow cytometry (excitation wavelength 488 nm, emission filter 585/42nm) using a FACS Calibur system. MDC has been reported to be a specific marker to label autophagic vacuoles.²² In brief, the cells were incubated with 0.05 mM MDC in PBS at 37°C for 10 minutes. After incubation, the cells were washed twice with PBS and intracellular MDC was visualized with a BX41 system microscope. 20,000 cells per sample were processed for flow cytometry (excitation wavelength 351–364 nm, emission filter 485/22nm) using a FACS Vantage system.

ATP quantitation

ATP was quantitated with a CellTiter-Glo Luminescent Cell Viability Assay kit (Promega Corporation). Luminescence was measured by Luminoskan Ascent from Thermo Scientific.

Quantitation of AMP, ADP and ATP by HPLC

700 μ l of 0.4 M perchloric acid and internal control were added into HCT116 cells after treatments. Cells were then frozen and thawed, and centrifuged. The pellets were used for protein measurements. The supernatant was neutralized with 1/10 volume of 4M K_2CO_3 and then centrifuged again. Supernatants were used for HPLC analysis. The HPLC analyses of AMP, ADP and ATP were performed on a Shimadzu LC-20AT HPLC system equipped with a Thermo scientific hypersil gold column (4.6 \times 150 mm, 3 μ m) preceded by a C18 precolumn cartridge. The solvent system comprised two buffers at a rate of 0.5 ml/min using an isocratic elution: 38% buffer B (V/V). Buffer A contained 25mM NaH_2PO_4 , 0.01% tetrabutylammonium hydroxide, pH 5. Buffer B was composed of 10% (V/V) acetonitrile in 200mM NaH_2PO_4 , 0.01% tetrabutylammonium hydroxide, pH 4.0. The compounds were detected by monitoring of UV absorbance at 254 nm, and they were quantified by comparison of peak areas to a standard curve. Protein measurements were performed using a BCA kit. Calculations were performed by peakheight calibrations and values were expressed as micromoles per gram wet weight or nanomoles per milligram of protein.

Flow cytometry for mitochondrial membrane potential detection

The mitochondrial membrane potential (ψ) of HCT116 cells after propionate treatment was measured using a Flow Cytometry Mitochondrial Membrane Potential Detection Kit (BD Biosciences). Fluorescence emission was analyzed by flow cytometry (JC-1 monomers: excitation wavelength 488nm, emission filter 530/30nm; JC-1 aggregates: excitation wavelength 488nm, emission filter 585/42 nm) using a FACS Calibur system. The ψ was also quantified by microscopic examination of cells stained with MitoTracker Deep Red FM and confirmed by flow cytometry analysis. In brief, the cell medium was aspirated after treatment, and MitoTracker Deep Red FM (100 nM in RPMI without FBS) was added for 15 min at 37°C. The fluorescence emission was either detected under microscope (BX41 fluorescence microscope from Olympus, Center Valley, PA) or analyzed by flow cytometry (excitation wavelength 635nm, emission filter 661/16nm).

Immunocytochemistry and Confocal Microscopy

HCT116 cells were seeded at 0.3×10^6 /well into 6-well plates with coverglasses to achieve 70% confluence. 36 hours later, the cells were treated with propionate (3mM) in the presence or absence of CQ (5 μ M) for 48 hours. The cells were fixed with 3% paraformaldehyde in PBS for 15 min, followed by permeabilization with 0.1% Triton X-100 for 5 min. After blocking in 3% BSA/1 \times PBS containing 3% horse serum for 40 min, the slides were incubated with COXIV/p62 or COXIV/LAMP2 antibodies at 4 °C overnight. After overnight incubation, the slides were washed three times with PBS and then incubated with Alexa Fluor® 568 goat anti-mouse IgG (H+L) and Alexa Fluor® 488 goat anti-rabbit IgG (H+L) secondary antibody for 1.5 h (1: 100 dilution). The slides were then washed three times with PBS, counterstained in Prolong® Gold antifade reagent with DAPI and visualized with an Olympus Fluoview confocal microscope using a 60 \times oil immersion objective lens (IX70 Olympus, Melville, NY, USA). Fluorescence was excited by the 488-nm line of an argon laser and the 568/647-nm line of a Krypton laser. Images were analyzed using Fluoview software.

Staining and flow cytometry analysis of mitochondria mass, ROS and MPT

Mitochondrial mass was measured by MitoTracker Green FM. Mitochondrion staining by MitoTracker Green FM follows the same protocol as to MitoTracker Deep Red FM staining. The fluorescence emission was detected by flow cytometry (excitation wavelength 488nm, emission filter 530/30nm). ROS was measured using an Image-iT™ LIVE Green Reactive Oxygen Species Detection Kit (Molecular Probes, I36007). In brief, the cells were treated with propionate at various concentrations and incubated with carboxy-H₂DCFDA (25 μM in Hank's balanced salt solution) for 30 minutes at 37°C, protected from light. DCF fluorescence was measured with a FACS Calibur flowcytometry system (excitation wavelength 488 nm, emission filter 530/30nm). A MitoProbe™ Transition Pore Assay Kit was used for mitochondrial membrane permeability transition (MPT) detection. In brief, the cells were treated with propionate at various concentrations and incubated with calcein-AM (10 nM) and CoCl₂ (0.4 mM) for 15 min at 37°. After a wash with PBS, calcein-AM fluorescence was either examined under a fluorescence microscope or measured with a FACS Calibur flow cytometry system (excitation wavelength 488 nm, emission filter 530 nm).

RT-PCR and real-time PCR

The expression profile of genes regulating mitochondria biogenesis was evaluated by semiquantitative reverse transcriptase PCR (RT-PCR) and Real-time quantitative PCR. Genes of interest were amplified by PCR from cDNA with the primer pairs listed in table 2. The reactions were performed as described by Chen et al.²³

Cell viability and apoptotic cell death measurement

For the MTS assay, 0.5×10^5 cells/well were plated in 96-well plates in RPMI medium, and the indicated drug treatments were applied 36 hours after seeding. At 48 hours, the MTS reagent supplied in CellTiter 96 AQueous Assay (Promega) was added. Cell viability was measured with Vi-CELL™ Series Cell Viability Analyzers (Beckman Coulter, Inc.), which is based on traditional cell viability method of trypan blue exclusion. In addition, a Vybrant Apoptosis Assay Kit (V35116), which provides a rapid and convenient assay for apoptosis based on PS translocation and changes in ψ , was used. MitoTracker Red and Alexa Fluor® 488 annexin V fluorescence were measured with a FACS Calibur flowcytometry system (MitoTracker Red: excitation wavelength 488nm, emission filter 585 nm; Alexa Fluor® 488 annexin V: excitation wavelength 488 nm, emission filter 530 nm).

Animal study

For each mouse, a total of 3×10^6 HCT116 cells infected with either random shRNA or shRNA against *ATG5* were injected s.c. into the right flank of 4- to 6-week-old male athymic nu/nu mice (Harlan Laboratories, Indianapolis, IN). The resulting palpable tumors were measured using a vernier caliper, and tumor volume was calculated using the formula: $\text{Vol} = (\text{Width})^2 \times \text{Length} \times 0.5$.

Statistics

The probability of statistically significant differences between two experimental groups was determined by Student's t-test. $P < 0.05$ was considered statistically significant in all calculations.

Results

Induction of autophagy by propionate in colon cancer cells

SCFAs, particularly propionate and butyrate, are well known for their antitumor effects toward colon cancer.^{4,5,24} In agreement with these reports, propionate and butyrate exhibited cytotoxicity toward colon cancer cell lines HCT116 and SW480. The IC_{50} value of propionate was 9 mM (HCT116) and 20 mM (SW480) while butyrate was more cytotoxic with an IC_{50} of 5 mM (Supplementary Figure S1).

During autophagy, the redistribution of GFP-LC3 to easily visualized “puncta” is a commonly used technique to monitor the autophagosome formation in living cells.¹⁹ In a PBS-treated control group, infected HCT116 cells predominantly displayed diffuse cytoplasmic GFP-LC3; propionate exposure prominently triggered the formation of characteristic punctate GFP-LC3, suggesting the recruitment of GFP-LC3 during autophagosome formation (Figure 1a). Treatment with propionate (3mM) resulted in a 10-fold increase in the percentage of cells with punctate GFP-LC3 compared with cancer cells treated with PBS by 36 hours (Figure 1bi). Propionate caused autophagy in a time-dependent manner (Figure 1bii). Lysosomal-associated membrane protein 2 (LAMP-2), an important constituent of the lysosomal membrane, has been reported to be critical for the lysosomal degradation of autophagic vacuoles.^{25,26} In this study, propionate caused an extensive upregulation of LAMP-2 expression (Figure 1c and Supplementary Figure S2a). The upregulated LAMP-2 displayed punctate structures and colocalized with propionate induced GFP-LC3 dots, which indicates the autolysosomes formation. The formation of punctate GFP-LC3 after propionate treatment was not confined to HCT116 cells but was also observed in SW480 cells with stable GFP-LC3 expression (Supplementary Figure S2d and e). Another SCFA butyrate, was also found to be able to induce autophagy in both HCT116 and SW480 cells in a manner similar to propionate (Data not shown).

During autophagosome formation, nascent LC3 is processed into soluble form LC3-I, which is further modified to form autophagosomal membrane-incorporated LC3-II,¹⁹ and the latter protein can be separated from the nonconjugated form (LC3-I) and detected by immunoblotting.²⁷ Immunoblot analyses revealed the presence of LC3-II after propionate treatment, and the level of LC3-II reached the highest level by 3mM propionate treatment (Figure 1ei). The degree of LC3-I to LC3-II conversion was initially low (as early as 6 hours posttreatment with propionate) but significantly enhanced thereafter (Figure 1eii). In addition to endogenous LC3, GFP-LC3 processing can be used to monitor the delivery of autophagosomal membranes.²⁸ In HCT116 with stable GFP-LC3 expression, the GFP-LC3-II level was dramatically increased following propionate treatment (Figure 1ei and ii). The increased total GFP-LC3 level was later confirmed by flow cytometry analysis to detect the mean of the GFP fluorescence value (Figure 1f). Aside from LC3, p62/SQSTM1, another

biochemical signs of autophagy,²⁹ was reduced (Figure 1d, Figure 1e, ii and Supplementary Figure S2b). On the other hand, the level of ATG7, which is essential for autophagosome formation, was upregulated. Upregulated LAMP-2 was also detected by western blot (Supplementary Figure S2c). Propionate also increased the conversion of LC3-I to LC3-II and of GFP-LC3-I to GFP-LC3-II and reduced the p62 level in SW480 cells (Supplementary Figure S2g).

Cells undergoing autophagy generally develop double-membraned, acidic vesicular organelles (autophagosomes), which can be detected by specific dyes. To this end, we used LysoTracker Red dye DND-99 (a dye detecting low pH) and MDC to label autophagic vacuoles. Treatment of HCT116 cells with increasing concentrations of propionate resulted in a progressive increase in LysoTracker or MDC-stained autolysosome-like structures, which resembled punctates (Figure 1a and 1f). Furthermore, GFP-LC3 punctates were largely colocalized with LysoTracker and MDC staining, indicating the formation of autolysosomes. Similar phenomena were also observed in cells placed under serum starvation, a condition that is well known to induce autophagy (Figure 1a). AVOs were quantified by flow cytometry (Figure 1f). The formation of autophagic vacuoles peaked at a propionate treatment with a concentration of 3mM and could not be further promoted by increasing the propionate concentration (Figure 1f). Propionate also increased the number of autophagic vacuoles in SW480 cells (Supplementary Figure S2d and f). Taken together, we conclude that an abundance of cytoplasmic acidic vesicular organelle formation, which is characteristic of autophagy, occurred in propionate treated cells.

Because LC3-II is subject to lysosomal degradation during autophagy, increased LC3-II levels do not always accurately reflect full-fledged autophagy induction. Instead, LC3-II accumulation could occur when downstream protein degradation is impaired. To assess autophagic flux more precisely, we assessed the accumulation of LC3-II in the presence of lysosomotropic agent chloroquine (CQ), which blocks the last critical step in autophagy, the acid-dependent degradation of autophagosome contents; and thereby results in the accumulation of autophagic vesicles that cannot be cleared.^{30,31} Combination treatment with propionate and CQ resulted in the accumulation of LC3-positive vesicles and caused more than a 10 fold increase in punctate LC3 fluorescence after 24 hours (Figure 1a and f). A further accumulation of LC3-II, GFP-LC3-II and p62 was detected (Figure 1c and eiii). Prevention of lysosome acidification by CQ resulted in the accumulation of punctate LAMP-2 (Supplementary Figure S2a and c). We also found that CQ substantially promoted the accumulation of acidic vesicular organelles (Figure 1a and f). Taken together, these observations further support the conclusion that propionate-mediated increase in LC3-II expression was a consequence of accelerated autophagosome formation, rather than impaired lysosomal clearance.

Propionate induced autophagy activation is associated with mTOR pathway inhibition

Autophagy regulation is a complex process that depends on a spectrum of factors. It is well established that the mammalian target of rapamycin (mTOR) negatively regulates autophagy.³² mTOR autophosphorylation at Ser2481 is regarded as an indicator for its catalytic activity.³³ As demonstrated by Western blot analysis, propionate exposure caused a

strong time-dependent reduction in the phosphorylation state of mTOR at Ser2481, while the total mTOR level was not changed noticeably (Figure 2). Next, we assessed the phosphorylation status of two key downstream effectors of mTOR: eukaryotic initiation factor 4E-binding proteins (4E-BP1) and p70 ribosomal S6 kinase (p70S6K), both of which are widely used as “readouts” for mTOR activity.^{34,35} Immunoblotting analysis revealed a clear decrease in 4E-BP1 phosphorylation in a dose- and time-dependent manner (Figure 2). To confirm this observation, we analyzed the phosphorylation status of the other major mTOR substrate p70S6K, whose phosphorylation status at Thr389 has been described to reflect mTOR activity,³⁶ while phosphorylation at Thr421/Ser424 is thought to activate p70S6K via relief of pseudo substrate suppression.³⁷ In agreement with the results on 4E-BP1 phosphorylation, protein dephosphorylation of p70S6K at Thr389 was noted by 7 hours following propionate treatment, and by 25 hours, a measured 3-fold decrease in the ratio of p70S6K (P-Thr389) to total p70S6K was observed (Figure 2). The level of p-p70S6K on Thr421/Ser424, showed a pattern similar to p-p70S6K on Thr389. We also found that the phosphorylation of mTOR at Ser-2448, which was reported to be the target of p70S6 kinase,³⁸ was reduced as well. Propionate also inhibited mTOR pathway in SW480 cells (Supplementary Figure S3). Collectively, these observations confirmed that downregulation of the mTOR signaling pathway is a mechanism for propionate to induce autophagy.

SCFA downregulation of mTOR pathway is associated with AMPK pathway activation

To characterize the molecular mechanisms underlying the reduced mTOR activation and concomitant autophagy induction by SCFA, we investigated the activation status of upstream signaling events involved in mTOR regulation. Of note, two separate pathways leading to the activation of mTOR has been well established: the oncogenic Akt/protein kinase B-PI3K pathway, which activates mTOR in response to the introduction of nutrient and growth factors, and the AMP-activated protein kinase (AMPK) pathway, which inhibits mTOR activity in response to metabolic stress signals such as nutrient starvation-induced cellular ATP depletion.³⁹⁻⁴¹ We next tested whether mTOR signaling activation is induced through the PI3K-Akt pathway. For this purpose, we assessed several major regulators of the pathway: class I PI3-kinases and class III PI3-kinase, which are distinct classes of PI3K that control the macroautophagic pathway in opposite directions;⁴² Akt, whose phosphorylation occurs at site Thr308 or at Ser⁴⁷³ is considered as an indicator of Akt activity,⁴³ while PTEN has a phosphatase activity which makes its cellular level inversely associated with Akt activity. Immunoblot analysis did not detect any noticeable difference in the phosphorylation of Akt at either Thr³⁰⁸ or Ser⁴⁷³, and the expression level of class I/III PI3-kinases (Figure 3a). The level of non-phosphorylated Akt was not changed either. In fact, a slight but consistent decrease in PTEN expression was observed (Figure 3a). The data suggest that the down-regulation of this major survival signaling pathway (PI3K-Akt) is not involved in propionate-induced mTOR pathway inhibition.

The above findings prompted us to analyze whether AMPK signaling pathway activation is responsible for mTOR pathway inhibition during propionate treatment. As a primary sensor of cellular bioenergetics, the AMPK-mediated signaling pathway has been described to sense the intracellular energy status and to regulate metabolism for maintaining cellular homeostasis, which plays a pivotal role in the cell's response to energy depletion.⁴⁴ More

importantly, AMPK has been reported to be a positive regulator of autophagy.⁴⁵ Phosphorylation of AMPK at the α subunit at threonine 172 (Thr¹⁷²) in response to an increased AMP to ATP ratio has been shown to be required for the activation of all known AMPK homologues.^{46,47} Propionate increased the phosphorylation level of AMPK α in HCT116 cells as early as seven hours following propionate treatment (Figure 3b). Additionally, despite the report that phosphorylation of either Thr²⁵⁸ or Ser^{485/491} does not cause any detectable activation of AMPK,⁴⁷ we still observed an elevation in the phosphorylation of AMPK α at Ser⁴⁸⁵ for α 1 and Ser⁴⁹¹ for α 2 (Figure 3b). Phosphorylation of one direct downstream target of AMPK, acetyl-coenzyme A carboxylase (ACC),⁴⁸ was detected. Propionate also increased AMPK α phosphorylation at Thr¹⁷² in SW480 cells (Supplementary Figure S4).

AMPK exists in cells as a heterotrimeric complex composed of a catalytic kinase subunit (α) and two regulatory subunits (β and γ). The presence of β/γ subunits contributes to the stability of the α subunit, helps prevent the auto-inhibitory domain with its active site, and enhances the allosteric activation (Thr¹⁷² phosphorylation) by AMP.⁴⁹ Contrary to the increased phosphorylation at Thr¹⁷² of the α subunit, propionate dramatically diminished the phosphorylation level of the AMPK β subunit at both Ser¹⁸¹ and Ser¹⁸², especially at a high concentration (10mM) (Figure 3b). In addition, AMPK γ -1 was reduced as well (Figure 3b). Whether the decreased β 1 subunit phosphorylation and γ expression play a part in the regulation of AMPK during propionate treatment awaits further investigation.

Consistent with the role of AMPK in down-regulation of mTOR signaling activity, propionate mediated inhibition of p70S6 kinase phosphorylation was markedly less pronounced in cells transfected with AMPK α shRNA (Figure 3c). Propionate-triggered autophagy induction was also impaired in AMPK α shRNA-infected cells, thus confirming that AMPK activation was a principal mechanism underlying these events (Figure 3c). Taken together, we conclude that the propionate-mediated autophagy induction in HCT116 and SW480 cells is based on AMPK pathway activation, instead of a decrease in PI3K-Akt signaling, and subsequent down-regulation of mTOR.

Propionate-induced AMPK signaling activation is associated with mitochondrial defect-induced cellular ATP depletion and oxidative stress

The data described above show that propionate inhibited the mTOR pathway by causing AMPK activation. AMPK is exquisitely sensitive to changes in the concentration of ATP.⁵⁰ We therefore attempted to ascertain whether AMPK activation by propionate is caused by cellular ATP reduction. Figure 4a shows that after an acute increase starting from 30 minutes and lasting for up to 5 hours, the intracellular ATP level declined steadily in HCT116 cells following propionate treatment. Propionate induced ATP reduction and AMP/ADP upregulation was further evaluated by HPLC (Supplementary Figure S5a). A similar ATP fluctuation pattern following propionate treatment was also observed in SW480 cells (Supplementary Figure S5b).

Depletion of energy sources or defective cellular energy generation would cause ATP depletion. Under normal conditions, mitochondria generate majority cellular ATP. Therefore, we next investigated whether the reduced cellular ATP during propionate

treatment is achieved through reduced mitochondria mass, impaired mitochondria functionality or both. Propionate led to depolarization of mitochondrial membrane as reflected by increased numbers of JC-1 stained cells, with reduced JC-1 fluorescence in the lower red fluorescence signal intensity (FL-2 axis) (Figure 4bi). In addition to JC-1, we also used MitoTracker® Deep Red, which stains mitochondria in live cells and accumulates in proportion to the membrane potential, to monitor ψ . Flow cytometry allowed identification of two populations of cells with distinct MitoTracker Deep Red staining intensities (Figure 4ci, and ii). The proportion of mitochondria with the lower fluorescence intensity, which reflected the depolarized mitochondria, was increased by propionate in a dose and time dependent manner (Figure 4ciii).

The loss of ψ may be caused by increased mitochondrial membrane permeability transition (MPT).⁵¹ To test whether an induction of MPT was involved with propionate-mediated reduction in ψ , HCT116 cells were treated with propionate and the MPT was detected based on an established method involving fluorescence staining with MitoTracker Deep Red, calcein-AM, and CoCl_2 .^{52,53} As shown in figure 4d, calcein was retained in untreated cells and colocalized with MitoTracker Deep Red-labeled mitochondria. However, propionate treatment led to loss of mitochondrial calcein fluorescence, which was due to calcein leakage from the mitochondria and was quenched by the subsequent addition of CoCl_2 . Additionally, reduced calcein fluorescence was associated with a concurrent reduction in MitoTracker deep red signals (Figure 4ei), which suggested that the loss of ψ was observed subsequent to continuous pore activation. The induction of MPT was partially blocked by cyclosporine A (Figure 4e), a reported MPT inhibitor which acts by binding cyclophilin D.⁵⁴ Altogether, these data suggest that the loss of ψ was associated with induction of MPT by propionate treatment.

Elevated ROS generation has been reported following MPT induction.⁵⁵ In fact, the fermentation products of *Propionibacterium*, propionate and acetate have been identified to enhance ROS generation in human colorectal carcinoma cell lines.⁵⁶ We measured the cellular ROS level by using Carboxy- H_2DCFDA , a fluorogenic marker for ROS in live cells.⁵⁷ Following propionate treatment, the percentage of cells positively stained for carboxy-DCF was increased (Figure 4f and g). When the cells were pretreated with the antioxidant N-acetylcysteine (NAC), ROS production was substantially inhibited. We also noticed that the cells positively stained with carboxy-DCF were those with impaired mitochondria membrane potential as reflected by reduced MitoTracker Red staining (Figure 4h). The observations suggested that the source of ROS production during propionate treatment is likely originated from defective mitochondria. In addition to increased AMP/ATP ratio, ROS serve as signaling molecules to activate AMPK.⁵⁸ The excessive ROS production has been suggested to play a role in the initiation of autophagy.^{57,59} Hence, the ant-oxidative effect of NAC on propionate mediated autophagy was examined. Antioxidant agent NAC inhibited the propionate induced ROS accumulation (Figure 4f and g) and attenuated the autophagy induction subsequently (Supplementary Figure S5c), providing evidence that ROS might contribute to the onset of autophagy. Cyclosporin A, which could attenuated MPT and reduced the release of ROS (data not shown), was also able to alleviate propionate triggered ROS accumulation and subsequent autophagy responses

(Supplementary Figure S5c). We were, however, unable to completely prevent the autophagic response by NAC or cyclosporin A, suggesting that ROS-independent autophagy was also being induced by propionate.

Malfunctioning mitochondria is selectively targeted for autophagic degradation.⁶⁰ Because of this, we suspected whether an alternative possibility that reduced cellular ATP production was being caused by a decrement in the mitochondrial mass. We used MitoTracker Green FM, which localizes to mitochondria regardless of ψ , to measure mitochondrial mass. A slight increase in by MitoTracker Green fluorescence was detected 12 hours after propionate exposure (Figure 4c). Taken together, the findings suggest that the decline in intracellular ATP during propionate treatment be attributed to the loss of ψ rather than to a decrease in mitochondria mass.

Defective Mitochondria are targeted for autophagic degradation

Autophagic degradation selectively targets depolarized mitochondria for digestion and elimination, a specific process also termed “mitophagy”, whose purpose is to rid the cell of damaged mitochondria and help prevent the activation of apoptotic pathways.⁶⁰ We used MitoTracker Deep Red to characterize the kinetics of mitochondria depolarization and mitophagy. As demonstrated in figure 5a, in untreated cells we observed the existence of a punctuate mitochondria distribution. However, in HCT116 cells undergoing propionate induced autophagy, we observed smeared mitochondria staining with dramatically reduced staining intensity and increased colocalization between mitochondria and punctate GFP-LC3. Propionate caused increased colocalization between punctate GFP-LC3 and mitochondria was also confirmed by the staining of COXIV (figure 5b). The autolysosomes localized defective mitochondria were also supported by increased colocalization between COXIV, a subunit of Complex IV localized in the mitochondrial inner membrane, and LAMP-2 (figure 5c). Increased colocalization between COXIV and a ubiquitin-binding protein-p62, which interacts with LC3 and regulates autophagosome formation,⁶¹ was also observed (Figure 5d). Blockage of autophagic degradation by CQ resulted in an accumulation of mitochondrial aggregates which overlap with LAMP-2 and p62 aggregates.

Propionate triggered mitophagy was supported by flow cytometry analysis which showed that the proportion of cells with reduced used MitoTracker Deep Red staining and enhanced GFP-LC3 fluorescence increased significantly following propionate treatment (Figure 5di). Termination of autophagic degradation by CQ dramatically increased the accumulation of defective mitochondria (Figure 5dii). The findings indicate that mitophagy selectively targets mitochondria with a depolarized membrane potential.

Rescue of cellular energy crisis through mitochondria biogenesis and alteration of glycogen and lipid metabolic pathways

AMPK provides a finely tuned amplification mechanism for energy homeostasis under conditions of low nutrient availability by shutting off of ATP-consuming anabolic pathways and up-regulating ATP-producing catabolic pathways.⁶² In this way, AMPK activation could restore the perturbation of cellular energy levels. In this study, propionate reduced the expression of fatty acid synthase (Figure 6a), which stores energy by catalyzing the

synthesis of long-chain fatty acids (LCFAs) from acetyl-CoA and malonyl-CoA. We also found that GSK-3 β , which inhibits endergonic glycogen synthesis by phosphorylation and inactivation of glycogen synthase, was down-regulated (Figure 6a). Furthermore, inactivation of ACC by AMPK mediated phosphorylation (Figure 3b), potentially inhibits *de novo* lipid synthesis,^{48,63} whereas inactivated ACC increases the mitochondrial import and oxidation of LCFAs, resulting in the generation of ATP.⁶⁴

Energy deprivation stimulates mitochondrial biogenesis in skeletal muscle in an AMPK-dependent manner.⁶⁵ Mitochondrial biogenesis requires relevant transcription factors to coordinate the expression of mitochondrial genes in two independent genomes. We examined several mitochondrial biogenesis markers that are pivotal in coordinating transactivation genes for OXPHOS protein expression/importation, and heme biosynthesis.⁶⁶ The expression of these genes at the mRNA level in HCT116 cells during propionate treatment was examined. As depicted in figure 6b and c, exposure of the cells to propionate stimulated Tfam and mtTFB expression at the mRNA level, peaking at 8.5 and 11.5 h, respectively, followed by a return to pre-stimulatory levels. Coordinately, NRF-1 and -2 and pol- γ expression at the mRNA level were also stimulated as early as 12 hours after treatment but were reduced after long term treatment. In contrast to the upregulation of these genes, we observed a time-dependent reduction in PGC-1 transcription (Figure 6b, c).

To ascertain whether mitochondrial biogenesis was truly induced, we examined the protein level of the mitochondrial redox carriers' subunits. The expression of a number of complex subunits located on the mitochondrial membrane was increased 8 hours post treatment, followed by a return to pre-stimulatory levels after 20 hours (Figure 6d). The alpha subunit of ATP synthase, which is a component of the F1 subcomplex of the proton-pumping ATPase responsible for ATP production in oxidative phosphorylation, was especially increased. The stimulation of mitochondrial biogenesis was also substantiated by an increase in MitoTracker Green FM fluorescence shown in Figure 4c. Altogether, the data suggest that HCT116 cells adapted to propionate-induced ATP depletion by down-regulating anabolic processes such as glycogen and lipid synthesis, while stimulating mitochondrial biogenesis in attempt to resume cellular energy homeostasis.

Propionate modulated autophagy induction and mTOR inhibition is independent of p53

The p53 tumour suppressor has a dual role in autophagy regulation.⁶⁷ In addition, several studies proposed that multiple cellular stressors activate p53 and stimulate autophagy through the involvement of AMPK-dependent mTOR inhibition.⁶⁸ To better define the role of p53 in propionate induced autophagy activation, we compared p53^{+/+} and p53^{-/-} HCT116 cell lines. A p53-deficient HCT116 cell line has been shown spontaneously activated cytoplasmic accumulation of autophagosomes.⁶⁸ However, we did not observe a noticeable difference as to the basal level autophagic flux between p53^{+/+} HCT116 and p53^{-/-} HCT116 cell lines judged both on the visible GFP-LC3 cytoplasmic puncta and GFP-LC3-II by Western blot (Figure 7a and b). We reasoned that the divergence exists because Ezgi Tasdemir and coworkers used plasmid-mediated GFP-LC3 expression, whereas in our study stable GFP-LC3 expression was achieved through a retrovirus mediated approach. Propionate was able to induce punctate GFP-LC3 formation and acidic

vacuole accumulation (Figure 7a and c). Increased conversion of LC3-I to LC3-II and GFP-LC3-I to GFP-LC3-II and degradation of p62 occurred in a time-dependent manner (Figure 7b). In addition, we observed that increased autophagic activity coincided with elevated AMPK phosphorylation and inhibited phosphorylation of the two mTOR downstream effectors p70S6 Kinase and 4E-BP1 (Figure 7d). Elevated AMPK phosphorylation was also associated with depletion of cellular ATP (data not shown). Importantly, the p53 level remained almost constant at the early stage following propionate treatment in both HCT116 and SW480 cells, both of which have wild-type p53 (Figure 7e). The p53 independent pattern of propionate induced autophagy is also supported by the fact that propionate is able to induce autophagy in SW480 cells, those express a *p53* gene harboring two point mutations.⁶⁹ These results demonstrated that p53 is not required for propionate-induced autophagy activation.

Inhibition of autophagy potentiates propionate-induced apoptotic cell death

Previous studies have highlighted the importance of SCFAs in colon cancer prevention in inducing caspase-3 mediated apoptosis.⁴ To shed light on the interconnection between propionate induced autophagy and apoptosis, the autophagy inhibitors were applied to examine the cell viability of HCT116 and SW480 cells during propionate treatment. 3-MA is a specific autophagy inhibitor that inhibits the earliest stages of autophagosome formation by abrogating Class III PI3-kinase activity.⁷⁰ The punctate GFP-LC3 formation observed in the cells treated with propionate was significantly reduced in cells pretreated with 3-MA at 2 mM (Figure 8a and b). At 24 and 48 hours, combined treatment with 3-MA significantly enhanced the cytotoxic effect of propionate treatment (Figure 8c). To further characterize this cell death, phosphatidylserine (PS) based annexin V staining was performed to assess the number of cells undergoing apoptosis (Figure 8d). At 12 hours after the initiation of treatment, propionate/3-MA treatment resulted in a marked increase in annexin V positive cancer cells compared with cells treated with propionate alone. This difference persisted at 48 hours, when a 1.75-fold difference in the percentage of annexin V-positive tumor cells was observed. Propionate/3-MA treatment also markedly induced chromatin condensation, indicating apoptotic cell death during propionate treatment (data not shown). As an independent approach to reflect cancer cell apoptosis, immunoblots revealed increased cleavages of the proapoptotic caspase-7 and executioner caspase-3, which are critical mediators of the mitochondrial events of apoptosis,⁷¹ in cancer cell lysates obtained 24 hours after the initiation of propionate/3-MA treatment compared with those treated with propionate alone (Figure 8e). Prevention of autophagic degradation by adding chloroquine also enhanced apoptosis of HCT116 cells, especially at the later stage of treatment (48 hours) (Figure 8d and e). Additionally, to substantiate the role of AMPK in propionate-triggered autophagy, we investigated whether shRNA-mediated AMPK α silencing could resemble the effects of autophagy inhibition on propionate cytotoxicity. The shRNA-mediated down-regulation of AMPK α augmented the propionate toxicity toward HCT116 cells, as demonstrated by a decrease in cell viability (Supplementary Figure S6e). Altogether, these results suggest that autophagic response plays a protective role in impeding the propionate-elicited death of colon cancer cells.

To further verify the protective role of autophagy against propionate-induced death, autophagy was suppressed via knockdown of *ATG5*, which is essential for elongation of the autophagic isolation membrane by the formation of the ATG5-ATG12 complex during autophagy. Decreased ATG5 expression in cells transduced with shATG5 was confirmed by Western blot (Figure 8f) and increased tumorigenesis *in vivo* (Supplementary Figure S6a). *ATG5* depletion reduced the ability of propionate to induce GFP-LC3 punctae formation (Figure 8a and b) and potentiated its effectiveness in the induction of cell death (Figure 8c and g). Inhibited autophagy responses, enhanced cell death and caspase-3/7 cleavage were also observed in the HCT116 cells with decreased ATG7 expression by the RNA interference (Supplementary Figure S6b, c and d). Autophagy inhibition by either a pharmacological (3-MA or CQ) or genetic (*ATG5* shRNA) approach also potentiated propionate-triggered apoptosis in SW480 cells (Supplementary Figure S6f, g, and h). Compared with HCT116, CQ is more effective in potentiating propionate-induced apoptosis in SW480 cells.

3-MA and CQ at higher dosage may have detrimental side effects on tumor cell viability apart from inhibiting autophagy. To confirm the antineoplastic effect of 3MA and CQ depends on their ability to inhibit autophagy-based survival, propionate/3MA or propionate/CQ treatment of cancer cells was compared with those in which autophagy was genetically inhibited using shRNA against *ATG5* (shATG5). Cotreatment of 3MA or CQ did not further enhance cell death following propionate exposure in cells with ATG5 knockdown, as shown in figure 8c,g and Supplementary Figure S6f, g. Hence, the ability of 3-MA and CQ to potentiate propionate-induced cell death is based on their suppressive effects on autophagy.

Discussion

The antitumor activities of SCFAs, especially butyrate, in colon cancer have been extensively studied.^{24,72} In the present study, we provide evidence that one major product of SCFAs, propionate is a strong inducer of another type of cell death (Type II PCD) termed “autophagy” in the human colon cancer cell lines HCT116 and SW480. Autophagy induction was achieved by inhibition of its negative regulator, the mTOR pathway, which was accompanied by increased AMPK α activation. Activation of AMPK occurred due to the depletion of intracellular ATP associated with mitochondria defects induced (MPT and ψ). Defective mitochondria were the source of increased ROS generation and were targeted for autophagic clearance. In addition, mitochondrial biogenesis was initiated to recover cellular energy homeostasis.

Paradoxically, autophagy promoted the survival of propionate-treated cancer cells. Pharmacological inhibition of autophagy, either by 3-MA or CQ, inhibited cell survival. Such effects were similarly achieved through genetic knockdown of the essential autophagy genes *ATG5/7*. Concomitant administration of 3-MA or CQ in cancer cells with downregulated *ATG5* expression failed to further enhance cell death following propionate treatment. This study provides evidence that autophagy is an adaptive mechanism that contributes to both survival of colon cancer cells and resistance to propionate-induced apoptosis. It underscores a rationale for further investigations on the use of autophagy

inhibitors for potentiating the conventional antineoplastic effects of SCFAs in colon cancer therapy.

Previous studies have had paradoxical observations concerning the role of autophagy in tumor cell biology. Autophagy may accelerate tumor development if it is decreased.⁷³ Consistent with this finding, the identification of autophagy-associated tumor suppressor gene *BECN1* strongly supports the idea that suppression or deficiency of autophagy genes contributes to tumorigenesis.^{74–76} Mathew and colleagues have suggested a potential explanation for these observations in that autophagy may restrain tumorigenesis by maintaining genome stability, which is pivotal for coping with metabolic stress encountered by established aggressive tumors.⁷⁷ In contrast, mounting evidence demonstrates that autophagy provides intrinsic alternative energy sources and contributes to the survival of cancer cells during antineoplastic therapies or under austere conditions such as nutrient starvation, particularly in advanced solid tumors.¹¹ Hence, development of an autophagy antagonist with clinical application may be an attractive approach. Taken together, these non-mutually exclusive data indicates that autophagy both stimulates or prevents cancer dependent on the context of tumorigenesis.

The present studies were undertaken because a variety of clinical anticancer therapies had been shown to stimulate autophagy. The consequences of autophagy in determining the fate of cancer cells has diverged into two distinct directions, as sulphoraphane, arsenic trioxide and temozolomide treatments have suggested that autophagy is serving a survival function; while tamoxifen and resveratrol have manifested autophagy as an indispensable approach to inducing cell death in cancer cell lines that display resistance to apoptosis.^{10, 13–15, 78–82} All of this evidence indicates that the consequences of autophagy in cancer therapy rely on the microenvironment and physiologic contexts of the tumor. The data presented above demonstrate the autophagy is induced in response to propionate. Autophagy serves as an adaptive response since cotreatment with autophagy inhibitors or expression of shRNA directed against *ATG5/7* augmented propionate-induced cell death. Our data suggest that autophagy is an adaptive strategy allowing for augmented resistance to apoptotic stimuli triggered by SCFAs in colon cancer cells.

Autophagy is activated in response to various stress stimuli, including starvation, hypoxia, endoplasmic reticulum stress and oxidative stress. In this study, autophagy induction was dependent on downregulation of its negative regulator mTOR, whose inactivation was linked to hyperphosphorylation of the AMPK α . AMPK is exquisitely sensitive to changes in the concentration of ATP.⁵⁰ In addition to increased AMP/ATP ratio, ROS serve as signaling molecules to activate AMPK.⁵⁸ In this study, the ATP depletion and ROS accumulation may jointly initiate AMPK activation. SCFAs are oxidized through β -oxidation to provide an alternative energy source for colonocytes, which may account for the transient ATP upregulation (1–7 hours). Subsequently, a drop of cellular ATP occurred (after 7 hours), which preceded the initiation of the extensive mitochondria membrane potential loss (12 hours) (Figure 5Cii). The observed early-stage (7–12 hours) ATP depletion might be explained by the enhanced ATP consumption due to increased Na⁺/HCO₃⁻-cotransporter (NBC) and the Na⁺/H⁺-exchanger (NHE) activities after SCFAs treatment.¹⁷ Through autophagic degradation to recycle damaged cellular constituents,

autophagy aids in sustaining bioenergetic homeostasis.⁸³ The direct evidence addressing the role of autophagy in ATP recovery is that abrogation of autophagy induction by *ATG5* knockdown or blockage of autophagic degradation by CQ precipitated propionate-induced ATP depletion (Supplementary Figure S7 and 5). Based on these results, we reasoned that autophagy induced in response to propionate may provide the tumor cell with an alternative energy supply to allow for adaptive protein synthesis and help overcome the cellular energy crisis caused by mitochondria defects.

Autophagy promotes cell survival, not only by recycling cellular constituents to sustain bioenergetics, but also by liquidating damaged organelles and protein aggregates, whose accumulation following cellular stress can be cytotoxic for the cells. For example, constant ROS accumulation is inevitably involved in oxidative stress. It directly oxidizes and damages the immediate surrounding organelles where they are produced, such as mitochondria.⁸⁴ Persistence of this vicious cycle may trigger a transient increase in mitochondrial ROS production via ROS activation of MPT, a phenomenon termed “ROS-induced ROS release (RIRR)”.⁸⁵ In the present study, flow cytometry analysis provided strong evidence suggesting a correlation between MPT induction, loss of ψ , increased ROS generation and autophagy targeting malfunctioning mitochondria degradation in that propionate induced a loss of ψ (Figure 4b and c), while mitochondria with compromised membrane potentials showed increased cyclosporin A-sensitive MPT (Figure 4e), ROS generation (Figure 4g and h) and were targeted for autophagic degradation (Figure 5). In addition to eliminating damaged and superfluous mitochondria, autophagic degradation also accounts for the reduced p62 expression following propionate treatment (Figure 1d and e). In this study, p62 reduction was observed as early as 6 hours after propionate treatment and by 12 hours a measured 50% decrease was detected (Figure 1e). p62 functions as a central “garbage disposer” to manage the degradation of toxic, misfolded protein aggregates, of which p62 itself is a component.⁸⁶ p62/SQSTM1, through recruitment of LC3 to autophagosomes, is required for formation and degradation of autophagosome by autophagy. Impaired autophagy leads to accumulation of p62, damaged mitochondria, and ROS.⁸⁷ Persistence of p62 accumulation then triggers a positive amplifying loop for additional ROS generation and enhanced genomic instability, thereby promoting tumorigenesis.^{77, 88} In support of this notion, termination of propionate-induced autophagy by CQ resulted in an ineffective autophagosome degradation, which led to an accumulation of mitochondria with compromised membrane potential (Figure 5d) and increased p62 aggregation (Figure 1d), indicative of protein quality control failure. Meanwhile, the cellular ROS was dramatically increased (Supplementary Figure S8). These results emphasize the role of the mitochondrial depolarization as a key event in mitochondrial autophagy and strengthen the idea that the mitochondrial permeability transition is a determinant of mitophagy.⁸⁹ Our observations also reinforce the role of autophagy in the removal of damaged mitochondria (the main source of ROS generated by propionate) and the protection of cells from increased ROS levels.

As two mechanistically distinct programmed cell deaths, autophagy and apoptosis can be induced simultaneously, sequentially, or in a mutually exclusive manner in response to cellular stresses.^{15, 80, 90} In present study, autophagy activation was observed as early as 12

hours after the initiation of propionate treatment (Figure 1b and e), while caspase 7 and 3 cleavage indicated autophagy was also noticed (Figure 8e and Supplementary Figure S6h). In another word, propionate caused apoptosis is preceded by, or is concomitant with, activation of autophagy. Mitochondria may be central organelles integrating the two types of cell death in that the mitochondrial permeability transition has been proposed to designate the cell's destiny by adopting either autophagy or apoptosis.^{54, 89} Additionally, ROS have been reported to trigger both autophagy and apoptosis.⁵⁷ Mitochondria play a central role in apoptosis, as the release of proapoptotic factors is responsible for the initiation of mitochondria-mediated apoptosis.⁹¹ Autophagic degradation of defective mitochondria could retard the occurrence of apoptosis by circumventing the release of proapoptotic factors such as cytochrome c from the mitochondria and the activation of the apoptotic cascade.⁹² In addition to its role as a signaling hub regulated by autophagy for autophagic degradation, p62 is also involved in the caspase-8 related apoptotic pathway.⁹³ This suggests that p62 is critical for temporally orchestrating the balance between antiapoptotic signals, by facilitating autophagic degradation of toxic aggregates or by activating proapoptotic signal via caspase 8 and its downstream executor caspases. Alternatively, apoptotic cell death is enhanced when self-defensive autophagy is inhibited pharmacologically (3-MA or CQ) or genetically (knockout of autophagy genes).

As alluded to in the previous paragraph, propionate-mediated AMPK hyperphosphorylation may allow a relief of mTOR inhibition on autophagy induction. The protective role of AMPK in propionate-mediated tumor cell killing was supported by the fact that AMPK silencing mimicked CQ or ATG5/7 knockdown mediated increase in cell death (Supplementary Figure S6e). However, the increased cell death may not be totally attributed to inhibited autophagy considering that AMPK plays a pivotal role in the cells' response to energy depletion.⁴⁴ Inhibition of AMPK activation by AMPK inhibitor compound C failed to potentiate propionate-induced apoptosis (data not shown and Figure 8e). This may be due to the low concentration of compound C (5 μ m) applied for the experiments as we found that higher concentrations of compound C (10 μ m) itself caused widespread cell death, although the possibility that AMPK-independent mechanism could also inhibit mTOR signaling cannot be excluded.

Propionate and butyrate have been reported to have histone deacetylase (HDAC) inhibitor activities.⁹⁴ To determine the possibility of propionate/butyrate induced autophagy is via their HDAC inhibitor activities, we treated HCT116 cells with Trichostatin A (TSA), a well known histone deacetylase inhibitor. However, we did not observe any alteration in autophagy markers indicating the activation of autophagic responses (Supplementary FigureS9), which indicates propionate/butyrate induced autophagy is not based on their HDAC inhibitor activities. In contrast, TSA was able to increase the transcription of cyclin-dependent kinase inhibitor p21 in HCT116 cells (data not shown).

The link between diet and cancer is complex and difficult to unravel. Consumption of fiber-rich vegetables, fruit and whole grain cereals is highly recommended as foods that are rich in fibers have been suggested to inhibit colon cancer, small intestine cancer and even ovarian cancer and breast cancer.⁹⁵⁻⁹⁸ However, some types of fibers apparently enhance colon carcinogenesis.⁹⁹ The relevance of SCFAs, the major bacterial fermentation products

of fibers, to cancer is manifold. Short-chain fatty acids have been reported as antitumor agents which selectively induce differentiation, growth arrest, and apoptosis in colon cancer cells.^{5,24,72} The results presented suggest that spontaneously induced autophagy by SCFAs would increase the resistance and flexibility of colon cancer toward an adverse microenvironment and compromise the efficacy of SCFAs themselves in colon cancer prevention. Perhaps most important is the fact that our study provides a proof of principle for enhancing the antitumor activities of SCFAs by modulation of autophagic pathways. Combination regimens including CQ or drugs targeting other steps in the autophagy pathway with high fiber containing food may be a feasible and promising therapeutic approach for colon cancer.

Supplementary Material

Refer to Web version on PubMed Central for supplementary material.

Acknowledgments

The authors would like to thank Anna Travelstead for acquisition of flow cytometry data; Dr. Jayanta Debnath for giving the retrovirus based GFP-LC3 expression construct and LC3 antibody; and Dr. Bert Vogelstein (The Johns Hopkins University, Baltimore) for providing the p53 null HCT-116 cell lines. We also would like to thank Gregory T. Robbins for his review and critical proofreading.

Abbreviations used

SCFAs	Short-chain fatty acids
MDC	Monodansylcadaverine
CQ	Chloroquine
3-MA	3-Methyladenine
MPT	mitochondrial membrane permeability transition
ψ	mitochondrial membrane potential
AVOs	acidic vesicular organelles
LC3	microtubule-associated protein light chain 3
ROS	reactive oxygen species
NAC	N-acetylcysteine
HPLC	high performance liquid chromatography
DAPI	40-6-diamidino-2-phenylindole
LAMP-2	lysosomal associated membrane protein 2

References

1. Jemal A, Siegel R, Ward E, Hao Y, Xu J, Murray T, et al. Cancer statistics, 2008. *CA Cancer J Clin.* 2008; 58:71–96. [PubMed: 18287387]
2. Cook SI, Sellin JH. Review article: short chain fatty acids in health and disease. *Aliment Pharmacol Ther.* 1998; 12:499–507. [PubMed: 9678808]

3. Cummings JH. Colonic absorption: the importance of short chain fatty acids in man. *Scand J Gastroenterol Suppl.* 1984; 93:89–99. [PubMed: 6374878]
4. Hague A, Elder DJ, Hicks DJ, Paraskeva C. Apoptosis in colorectal tumour cells: induction by the short chain fatty acids butyrate, propionate and acetate and by the bile salt deoxycholate. *Int J Cancer.* 1995; 60:400–6. [PubMed: 7829251]
5. Ruemmele FM, Dionne S, Qureshi I, Sarma DS, Levy E, Seidman EG. Butyrate mediates Caco-2 cell apoptosis via up-regulation of pro-apoptotic BAK and inducing caspase-3 mediated cleavage of poly-(ADP-ribose) polymerase (PARP). *Cell Death Differ.* 1999; 6:729–35. [PubMed: 10467346]
6. Trock B, Lanza E, Greenwald P. Dietary fiber, vegetables, and colon cancer: critical review and meta-analyses of the epidemiologic evidence. *J Natl Cancer Inst.* 1990; 82:650–61. [PubMed: 2157027]
7. Klionsky DJ, Emr SD. Autophagy as a regulated pathway of cellular degradation. *Science.* 2000; 290:1717–21. [PubMed: 11099404]
8. Seglen PO, Bohley P. Autophagy and other vacuolar protein degradation mechanisms. *Experientia.* 1992; 48:158–72. [PubMed: 1740188]
9. Levine B, Klionsky DJ. Development by self-digestion: molecular mechanisms and biological functions of autophagy. *Dev Cell.* 2004; 6:463–77. [PubMed: 15068787]
10. Paglin S, Hollister T, Delohery T, Hackett N, McMahill M, Sphicas E, et al. A novel response of cancer cells to radiation involves autophagy and formation of acidic vesicles. *Cancer Res.* 2001; 61:439–44. [PubMed: 11212227]
11. Kondo Y, Kanzawa T, Sawaya R, Kondo S. The role of autophagy in cancer development and response to therapy. *Nat Rev Cancer.* 2005; 5:726–34. [PubMed: 16148885]
12. Amaravadi RK, Thompson CB. The roles of therapy-induced autophagy and necrosis in cancer treatment. *Clin Cancer Res.* 2007; 13:7271–9. [PubMed: 18094407]
13. Bursch W, Ellinger A, Kienzl H, Torok L, Pandey S, Sikorska M, et al. Active cell death induced by the anti-estrogens tamoxifen and ICI 164 384 in human mammary carcinoma cells (MCF-7) in culture: the role of autophagy. *Carcinogenesis.* 1996; 17:1595–607. [PubMed: 8761415]
14. Gozuacik D, Kimchi A. Autophagy as a cell death and tumor suppressor mechanism. *Oncogene.* 2004; 23:2891–906. [PubMed: 15077152]
15. Herman-Antosiewicz A, Johnson DE, Singh SV. Sulforaphane causes autophagy to inhibit release of cytochrome C and apoptosis in human prostate cancer cells. *Cancer Res.* 2006; 66:5828–35. [PubMed: 16740722]
16. Degenhardt K, Mathew R, Beaudoin B, Bray K, Anderson D, Chen G, et al. Autophagy promotes tumor cell survival and restricts necrosis, inflammation, and tumorigenesis. *Cancer Cell.* 2006; 10:51–64. [PubMed: 16843265]
17. Rodenburg W, Keijer J, Kramer E, Vink C, van der Meer R, Bovee-Oudenhoven IM. Impaired barrier function by dietary fructo-oligosaccharides (FOS) in rats is accompanied by increased colonic mitochondrial gene expression. *BMC Genomics.* 2008; 9:144. [PubMed: 18371188]
18. Fung C, Lock R, Gao S, Salas E, Debnath J. Induction of autophagy during extracellular matrix detachment promotes cell survival. *Mol Biol Cell.* 2008; 19:797–806. [PubMed: 18094039]
19. Kabeya Y, Mizushima N, Ueno T, Yamamoto A, Kirisako T, Noda T, et al. LC3, a mammalian homologue of yeast Apg8p, is localized in autophagosomal membranes after processing. *Embo J.* 2000; 19:5720–8. [PubMed: 11060023]
20. Rusten TE, Lindmo K, Juhasz G, Sass M, Seglen PO, Brech A, et al. Programmed autophagy in the *Drosophila* fat body is induced by ecdysone through regulation of the PI3K pathway. *Dev Cell.* 2004; 7:179–92. [PubMed: 15296715]
21. Scott RC, Schuldiner O, Neufeld TP. Role and regulation of starvation-induced autophagy in the *Drosophila* fat body. *Dev Cell.* 2004; 7:167–78. [PubMed: 15296714]
22. Munafò DB, Colombo MI. A novel assay to study autophagy: regulation of autophagosome vacuole size by amino acid deprivation. *J Cell Sci.* 2001; 114:3619–29. [PubMed: 11707514]
23. Chen Y, Tang Y, Wang MT, Zeng S, Nie D. Human pregnane X receptor and resistance to chemotherapy in prostate cancer. *Cancer Res.* 2007; 67:10361–7. [PubMed: 17974979]

24. Heerdt BG, Houston MA, Augenlicht LH. Potentiation by specific short-chain fatty acids of differentiation and apoptosis in human colonic carcinoma cell lines. *Cancer Res.* 1994; 54:3288–93. [PubMed: 8205551]
25. Tanaka Y, Guhde G, Suter A, Eskelinen EL, Hartmann D, Lullmann-Rauch R, et al. Accumulation of autophagic vacuoles and cardiomyopathy in LAMP-2-deficient mice. *Nature.* 2000; 406:902–6. [PubMed: 10972293]
26. Eskelinen EL, Illert AL, Tanaka Y, Schwarzmann G, Blanz J, Von Figura K, et al. Role of LAMP-2 in lysosome biogenesis and autophagy. *Mol Biol Cell.* 2002; 13:3355–68. [PubMed: 12221139]
27. Mizushima N, Yoshimori T. How to interpret LC3 immunoblotting. *Autophagy.* 2007; 3:542–5. [PubMed: 17611390]
28. Klionsky DJ, Abeliovich H, Agostinis P, Agrawal DK, Aliev G, Askew DS, et al. Guidelines for the use and interpretation of assays for monitoring autophagy in higher eukaryotes. *Autophagy.* 2008; 4:151–75. [PubMed: 18188003]
29. Komatsu M, Waguri S, Koike M, Sou YS, Ueno T, Hara T, et al. Homeostatic levels of p62 control cytoplasmic inclusion body formation in autophagy-deficient mice. *Cell.* 2007; 131:1149–63. [PubMed: 18083104]
30. Amaravadi, Ravi K.; DY; Lum, Julian J.; Thomas-Tikhonenko, Andrei; Thompson, Craig B. Inhibition of autophagy with chloroquine enhances therapeutic tumor regression in a mouse model of B cell lymphoma. *Proc Amer Assoc Cancer Res.* 2006; 47
31. Amaravadi RK, Yu D, Lum JJ, Bui T, Christophorou MA, Evan GI, et al. Autophagy inhibition enhances therapy-induced apoptosis in a Myc-induced model of lymphoma. *J Clin Invest.* 2007; 117:326–36. [PubMed: 17235397]
32. Mathew R, Karantza-Wadsworth V, White E. Role of autophagy in cancer. *Nat Rev Cancer.* 2007; 7:961–7. [PubMed: 17972889]
33. Peterson RT, Beal PA, Comb MJ, Schreiber SL. FKBP12-rapamycin-associated protein (FRAP) autophosphorylates at serine 2481 under translationally repressive conditions. *J Biol Chem.* 2000; 275:7416–23. [PubMed: 10702316]
34. Brugarolas J, Lei K, Hurley RL, Manning BD, Reiling JH, Hafen E, et al. Regulation of mTOR function in response to hypoxia by REDD1 and the TSC1/TSC2 tumor suppressor complex. *Genes Dev.* 2004; 18:2893–904. [PubMed: 15545625]
35. Inoki K, Zhu T, Guan KL. TSC2 mediates cellular energy response to control cell growth and survival. *Cell.* 2003; 115:577–90. [PubMed: 14651849]
36. Pullen N, Thomas G. The modular phosphorylation and activation of p70s6k. *FEBS Lett.* 1997; 410:78–82. [PubMed: 9247127]
37. Dufner A, Thomas G. Ribosomal S6 kinase signaling and the control of translation. *Exp Cell Res.* 1999; 253:100–9. [PubMed: 10579915]
38. Chiang GG, Abraham RT. Phosphorylation of mammalian target of rapamycin (mTOR) at Ser-2448 is mediated by p70S6 kinase. *J Biol Chem.* 2005; 280:25485–90. [PubMed: 15899889]
39. Arsham AM, Neufeld TP. Thinking globally and acting locally with TOR. *Curr Opin Cell Biol.* 2006; 18:589–97. [PubMed: 17046229]
40. Hardie DG. The AMP-activated protein kinase pathway--new players upstream and downstream. *J Cell Sci.* 2004; 117:5479–87. [PubMed: 15509864]
41. Dennis PB, Jaeschke A, Saitoh M, Fowler B, Kozma SC, Thomas G. Mammalian TOR: a homeostatic ATP sensor. *Science.* 2001; 294:1102–5. [PubMed: 11691993]
42. Petiot A, Ogier-Denis E, Blommaert EF, Meijer AJ, Codogno P. Distinct classes of phosphatidylinositol 3'-kinases are involved in signaling pathways that control macroautophagy in HT-29 cells. *J Biol Chem.* 2000; 275:992–8. [PubMed: 10625637]
43. Sarbassov DD, Guertin DA, Ali SM, Sabatini DM. Phosphorylation and regulation of Akt/PKB by the rictor-mTOR complex. *Science.* 2005; 307:1098–101. [PubMed: 15718470]
44. Kato K, Ogura T, Kishimoto A, Minegishi Y, Nakajima N, Miyazaki M, et al. Critical roles of AMP-activated protein kinase in constitutive tolerance of cancer cells to nutrient deprivation and tumor formation. *Oncogene.* 2002; 21:6082–90. [PubMed: 12203120]

45. Meley D, Bauvy C, Houben-Weerts JH, Dubbelhuis PF, Helmond MT, Codogno P, et al. AMP-activated protein kinase and the regulation of autophagic proteolysis. *J Biol Chem.* 2006; 281:34870–9. [PubMed: 16990266]
46. Hardie DG, Scott JW, Pan DA, Hudson ER. Management of cellular energy by the AMP-activated protein kinase system. *FEBS Lett.* 2003; 546:113–20. [PubMed: 12829246]
47. Stein SC, Woods A, Jones NA, Davison MD, Carling D. The regulation of AMP-activated protein kinase by phosphorylation. *Biochem J.* 2000; 345(Pt 3):437–43. [PubMed: 10642499]
48. Munday MR. Regulation of mammalian acetyl-CoA carboxylase. *Biochem Soc Trans.* 2002; 30:1059–64. [PubMed: 12440972]
49. Cheung PC, Salt IP, Davies SP, Hardie DG, Carling D. Characterization of AMP-activated protein kinase gamma-subunit isoforms and their role in AMP binding. *Biochem J.* 2000; 346(Pt 3):659–69. [PubMed: 10698692]
50. Hardie DG. Roles of the AMP-activated/SNF1 protein kinase family in the response to cellular stress. *Biochem Soc Symp.* 1999; 64:13–27. [PubMed: 10207618]
51. Ly JD, Grubb DR, Lawen A. The mitochondrial membrane potential ($\Delta\psi(m)$) in apoptosis; an update. *Apoptosis.* 2003; 8:115–28. [PubMed: 12766472]
52. Petronilli V, Miotto G, Canton M, Brini M, Colonna R, Bernardi P, et al. Transient and long-lasting openings of the mitochondrial permeability transition pore can be monitored directly in intact cells by changes in mitochondrial calcein fluorescence. *Biophys J.* 1999; 76:725–34. [PubMed: 9929477]
53. Petronilli V, Miotto G, Canton M, Colonna R, Bernardi P, Di Lisa F. Imaging the mitochondrial permeability transition pore in intact cells. *Biofactors.* 1998; 8:263–72. [PubMed: 9914828]
54. Lemasters JJ, Nieminen AL, Qian T, Trost LC, Elmore SP, Nishimura Y, et al. The mitochondrial permeability transition in cell death: a common mechanism in necrosis, apoptosis and autophagy. *Biochim Biophys Acta.* 1998; 1366:177–96. [PubMed: 9714796]
55. Kanno T, Sato EE, Muranaka S, Fujita H, Fujiwara T, Utsumi T, et al. Oxidative stress underlies the mechanism for Ca^{2+} -induced permeability transition of mitochondria. *Free Radic Res.* 2004; 38:27–35. [PubMed: 15061651]
56. Jan G, Belzacq AS, Haouzi D, Rouault A, Metivier D, Kroemer G, et al. Propionibacteria induce apoptosis of colorectal carcinoma cells via short-chain fatty acids acting on mitochondria. *Cell Death Differ.* 2002; 9:179–88. [PubMed: 11840168]
57. Scherz-Shouval R, Shvets E, Fass E, Shorer H, Gil L, Elazar Z. Reactive oxygen species are essential for autophagy and specifically regulate the activity of Atg4. *Embo J.* 2007; 26:1749–60. [PubMed: 17347651]
58. Emerling BM, Weinberg F, Snyder C, Burgess Z, Mutlu GM, Viollet B, et al. Hypoxic activation of AMPK is dependent on mitochondrial ROS but independent of an increase in AMP/ATP ratio. *Free Radic Biol Med.* 2009; 46:1386–91. [PubMed: 19268526]
59. Jin S. Autophagy, mitochondrial quality control, and oncogenesis. *Autophagy.* 2006; 2:80–4. [PubMed: 16874075]
60. Lemasters JJ. Selective mitochondrial autophagy, or mitophagy, as a targeted defense against oxidative stress, mitochondrial dysfunction, and aging. *Rejuvenation Res.* 2005; 8:3–5. [PubMed: 15798367]
61. Pankiv S, Clausen TH, Lamark T, Brech A, Bruun JA, Outzen H, et al. p62/SQSTM1 binds directly to Atg8/LC3 to facilitate degradation of ubiquitinated protein aggregates by autophagy. *J Biol Chem.* 2007; 282:24131–45. [PubMed: 17580304]
62. Rutter GA, Da Silva Xavier G, Leclerc I. Roles of 5'-AMP-activated protein kinase (AMPK) in mammalian glucose homeostasis. *Biochem J.* 2003; 375:1–16. [PubMed: 12839490]
63. Carling D. AMP-activated protein kinase: balancing the scales. *Biochimie.* 2005; 87:87–91. [PubMed: 15733742]
64. McGarry JD. Banting lecture 2001: dysregulation of fatty acid metabolism in the etiology of type 2 diabetes. *Diabetes.* 2002; 51:7–18. [PubMed: 11756317]
65. Zong H, Ren JM, Young LH, Pypaert M, Mu J, Birnbaum MJ, et al. AMP kinase is required for mitochondrial biogenesis in skeletal muscle in response to chronic energy deprivation. *Proc Natl Acad Sci U S A.* 2002; 99:15983–7. [PubMed: 12444247]

66. Suliman HB, Welty-Wolf KE, Carraway M, Tatro L, Piantadosi CA. Lipopolysaccharide induces oxidative cardiac mitochondrial damage and biogenesis. *Cardiovasc Res.* 2004; 64:279–88. [PubMed: 15485687]
67. Levine B, Abrams J. p53: The Janus of autophagy? *Nat Cell Biol.* 2008; 10:637–9. [PubMed: 18521069]
68. Tasdemir E, Maiuri MC, Galluzzi L, Vitale I, Djavaheri-Mergny M, D'Amelio M, et al. Regulation of autophagy by cytoplasmic p53. *Nat Cell Biol.* 2008; 10:676–87. [PubMed: 18454141]
69. Baker SJ, Markowitz S, Fearon ER, Willson JK, Vogelstein B. Suppression of human colorectal carcinoma cell growth by wild-type p53. *Science.* 1990; 249:912–5. [PubMed: 2144057]
70. Seglen PO, Gordon PB. 3-Methyladenine: specific inhibitor of autophagic/lysosomal protein degradation in isolated rat hepatocytes. *Proc Natl Acad Sci U S A.* 1982; 79:1889–92. [PubMed: 6952238]
71. Lakhani SA, Masud A, Kuida K, Porter GA Jr, Booth CJ, Mehal WZ, et al. Caspases 3 and 7: key mediators of mitochondrial events of apoptosis. *Science.* 2006; 311:847–51. [PubMed: 16469926]
72. Medina V, Edmonds B, Young GP, James R, Appleton S, Zalewski PD. Induction of caspase-3 protease activity and apoptosis by butyrate and trichostatin A (inhibitors of histone deacetylase): dependence on protein synthesis and synergy with a mitochondrial/cytochrome c-dependent pathway. *Cancer Res.* 1997; 57:3697–707. [PubMed: 9288776]
73. Okada H, Mak TW. Pathways of apoptotic and non-apoptotic death in tumour cells. *Nat Rev Cancer.* 2004; 4:592–603. [PubMed: 15286739]
74. Liang XH, Jackson S, Seaman M, Brown K, Kempkes B, Hibshoosh H, et al. Induction of autophagy and inhibition of tumorigenesis by beclin 1. *Nature.* 1999; 402:672–6. [PubMed: 10604474]
75. Aita VM, Liang XH, Murty VV, Pincus DL, Yu W, Cayanis E, et al. Cloning and genomic organization of beclin 1, a candidate tumor suppressor gene on chromosome 17q21. *Genomics.* 1999; 59:59–65. [PubMed: 10395800]
76. Qu X, Yu J, Bhagat G, Furuya N, Hibshoosh H, Troxel A, et al. Promotion of tumorigenesis by heterozygous disruption of the beclin 1 autophagy gene. *J Clin Invest.* 2003; 112:1809–20. [PubMed: 14638851]
77. Mathew R, Kongara S, Beaudoin B, Karp CM, Bray K, Degenhardt K, et al. Autophagy suppresses tumor progression by limiting chromosomal instability. *Genes Dev.* 2007; 21:1367–81. [PubMed: 17510285]
78. Ito H, Daido S, Kanzawa T, Kondo S, Kondo Y. Radiation-induced autophagy is associated with LC3 and its inhibition sensitizes malignant glioma cells. *Int J Oncol.* 2005; 26:1401–10. [PubMed: 15809734]
79. Kanzawa T, Germano IM, Komata T, Ito H, Kondo Y, Kondo S. Role of autophagy in temozolomide-induced cytotoxicity for malignant glioma cells. *Cell Death Differ.* 2004; 11:448–57. [PubMed: 14713959]
80. Kanzawa T, Kondo Y, Ito H, Kondo S, Germano I. Induction of autophagic cell death in malignant glioma cells by arsenic trioxide. *Cancer Res.* 2003; 63:2103–8. [PubMed: 12727826]
81. Opiari AW Jr, Tan L, Boitano AE, Sorenson DR, Aurora A, Liu JR. Resveratrol-induced autophagocytosis in ovarian cancer cells. *Cancer Res.* 2004; 64:696–703. [PubMed: 14744787]
82. Daido S, Kanzawa T, Yamamoto A, Takeuchi H, Kondo Y, Kondo S. Pivotal role of the cell death factor BNIP3 in ceramide-induced autophagic cell death in malignant glioma cells. *Cancer Res.* 2004; 64:4286–93. [PubMed: 15205343]
83. Codogno P, Meijer AJ. Autophagy and signaling: their role in cell survival and cell death. *Cell Death Differ.* 2005; 12(Suppl 2):1509–18. [PubMed: 16247498]
84. Balaban RS, Nemoto S, Finkel T. Mitochondria, oxidants, and aging. *Cell.* 2005; 120:483–95. [PubMed: 15734681]
85. Zorov DB, Filburn CR, Klotz LO, Zweier JL, Sollott SJ. Reactive oxygen species (ROS)-induced ROS release: a new phenomenon accompanying induction of the mitochondrial permeability transition in cardiac myocytes. *J Exp Med.* 2000; 192:1001–14. [PubMed: 11015441]

86. Zatloukal K, Stumptner C, Fuchsbichler A, Heid H, Schnoelzer M, Kenner L, et al. p62 Is a common component of cytoplasmic inclusions in protein aggregation diseases. *Am J Pathol.* 2002; 160:255–63. [PubMed: 11786419]
87. Moscat J, Diaz-Meco MT. p62 at the crossroads of autophagy, apoptosis, and cancer. *Cell.* 2009; 137:1001–4. [PubMed: 19524504]
88. Mathew R, Karp CM, Beaudoin B, Vuong N, Chen G, Chen HY, et al. Autophagy suppresses tumorigenesis through elimination of p62. *Cell.* 2009; 137:1062–75. [PubMed: 19524509]
89. Rodriguez-Enriquez S, He L, Lemasters JJ. Role of mitochondrial permeability transition pores in mitochondrial autophagy. *Int J Biochem Cell Biol.* 2004; 36:2463–72. [PubMed: 15325585]
90. Xue L, Fletcher GC, Tolkovsky AM. Mitochondria are selectively eliminated from eukaryotic cells after blockade of caspases during apoptosis. *Curr Biol.* 2001; 11:361–5. [PubMed: 11267874]
91. van Loo G, Saelens X, van Gurp M, MacFarlane M, Martin SJ, Vandenabeele P. The role of mitochondrial factors in apoptosis: a Russian roulette with more than one bullet. *Cell Death Differ.* 2002; 9:1031–42. [PubMed: 12232790]
92. Colell A, Ricci JE, Tait S, Milasta S, Maurer U, Bouchier-Hayes L, et al. GAPDH and autophagy preserve survival after apoptotic cytochrome c release in the absence of caspase activation. *Cell.* 2007; 129:983–97. [PubMed: 17540177]
93. Jin Z, Li Y, Pitti R, Lawrence D, Pham VC, Lill JR, et al. Cullin3-based polyubiquitination and p62-dependent aggregation of caspase-8 mediate extrinsic apoptosis signaling. *Cell.* 2009; 137:721–35. [PubMed: 19427028]
94. Aoyama M, Kotani J, Usami M. Butyrate and propionate induced activated or non-activated neutrophil apoptosis via HDAC inhibitor activity but without activating GPR-41/GPR-43 pathways. *Nutrition.* 2009
95. Jacobs LR. Dietary fiber and cancer. *J Nutr.* 1987; 117:1319–21. [PubMed: 3039088]
96. Silvera SA, Jain M, Howe GR, Miller AB, Rohan TE. Dietary fiber intake and ovarian cancer risk: a prospective cohort study. *Cancer Causes Control.* 2007; 18:335–41. [PubMed: 17285261]
97. Park Y, Hunter DJ, Spiegelman D, Bergkvist L, Berrino F, van den Brandt PA, et al. Dietary fiber intake and risk of colorectal cancer: a pooled analysis of prospective cohort studies. *Jama.* 2005; 294:2849–57. [PubMed: 16352792]
98. Mai V, Flood A, Peters U, Lacey JV Jr. Schairer C, Schatzkin A. Dietary fibre and risk of colorectal cancer in the Breast Cancer Detection Demonstration Project (BCDDP) follow-up cohort. *Int J Epidemiol.* 2003; 32:234–9. [PubMed: 12714542]
99. Jacobs LR. Relationship between dietary fiber and cancer: metabolic, physiologic, and cellular mechanisms. *Proc Soc Exp Biol Med.* 1986; 183:299–310. [PubMed: 3025886]

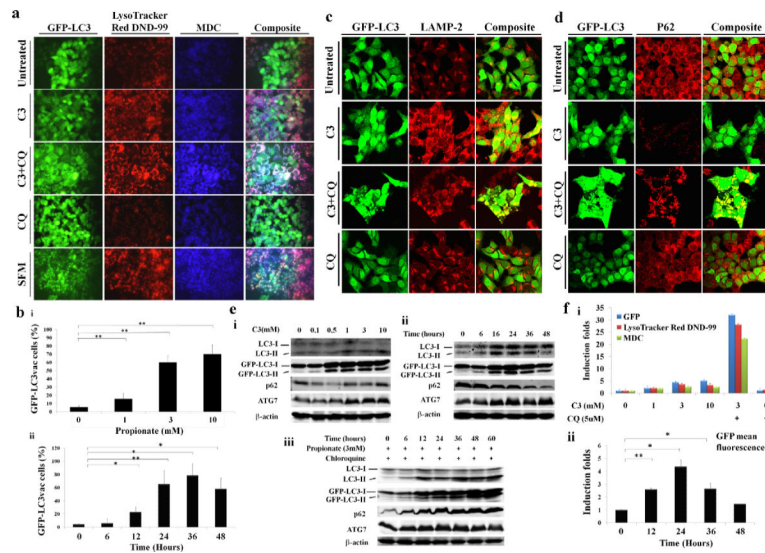


Figure 1. Induction of autophagy by propionate in colon cancer cells

(a) A bulk population of HCT116 cells with stable GFP-LC3 expression was treated with propionate (C3, 3mM) for 36 hours or was starved within serum free medium (positive control) for 24 hours. Cell culture medium was changed daily. Formation of acidic vesicular organelles was monitored by LysoTracker DND-99 or MDC staining. Chloroquine (CQ) (5uM) was added to increase the accumulation of autophagosomes. Representative images of cells were taken with a fluorescence microscope at 600 \times magnification. Note the pink color in a composite panel, which stands for the colocalization of punctate GFP-LC3, LysoTracker DND-99 and MDC staining.

(b) Quantification of the percentage of cells with more than 8 GFP-LC3 puncta per cell is represented as “GFP-LC3^{vac} cells (%)”. GFP-LC3 expressing cells were treated with indicated concentrations of propionate for 36 hours (i). The percentage of cells with punctate GFP-LC3 caused by 3mM propionate was monitored at different time points (ii). A minimum of 100 GFP-LC3 expressing cells were counted. *P < 0.01; ** P < 0.001, compared with PBS control at the corresponding time.

HCT116 cells were treated with propionate (3mM) in the presence or absence of CQ (5uM) for 24 hours. The cells were stained with LAMP-2 antibody (c) or p62 antibody (d). Representative images of cells were taken with an Olympus Fluoview confocal microscope using a 60 \times oil immersion objective lens.

(e) HCT116 cells with stable GFP-LC3 expression were subjected to propionate at different concentrations (i) or propionate (3mM) for the indicated times (ii). The cell lysates were immunoblotted against several autophagy markers. Autophagy markers were also examined in the cells treated with propionate in the presence of CQ (5uM) (iii).

(f) Increased acidic vesicular organelle formation was reflected by elevated punctate LysoTracker staining and increased MDC incorporation in HCT116 cells after propionate treatment. HCT116 cells were subjected to propionate at different concentrations (i) or propionate (3mM) for the indicated times (ii). The cells were stained with the dyes and subjected to flow cytometry analysis. The bars represent the mean \pm SE (n=4). *P < 0.01; ** P < 0.001, compared with PBS control at the corresponding time.

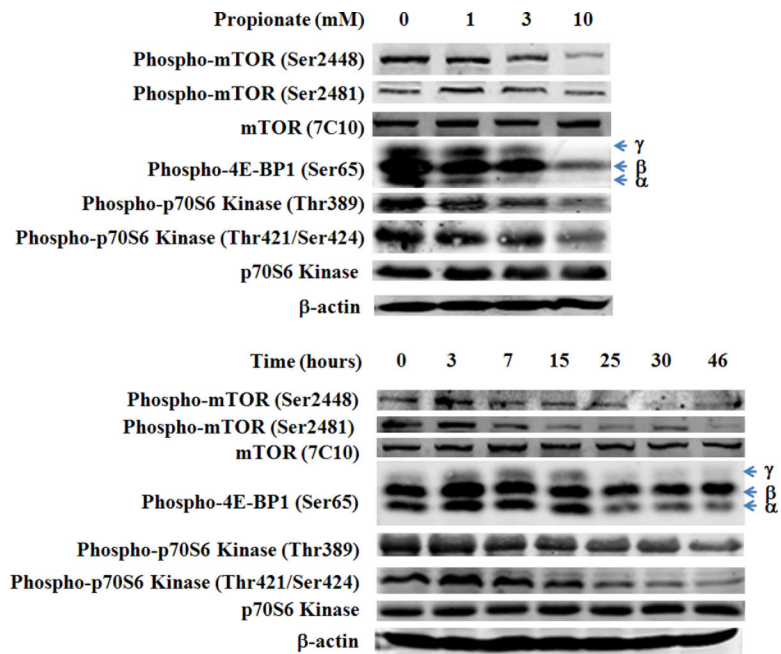


Figure 2. Propionate-induced autophagy activation is associated with mTOR pathway inhibition HCT116 cells were treated with propionate at different concentrations (top) for 15 hours or with 3mM propionate for the indicated time (bottom). The phosphorylation status of mTOR, and its major downstream substrates, 4E-BP1 and p70S6 Kinase, was detected by Western blot. As for 4E-BP1 phosphorylation, γ stands for the hyper-phosphorylated form of 4E-BP1, whereas β and α stand for medium- and low-phosphorylated forms of 4E-BP1. The data represent as least three independent experiments.

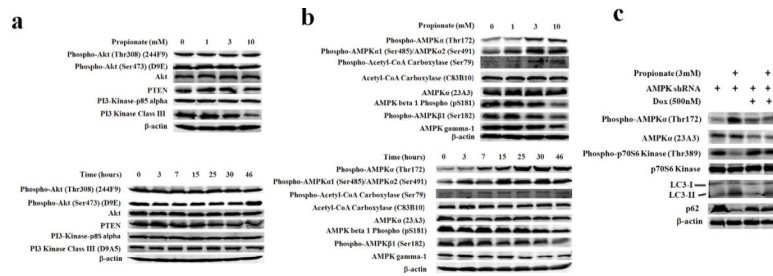


Figure 3. Induction of autophagy via inhibition of mTOR pathway is associated with AMPK pathway activation

HCT116 cells were treated with propionate at the indicated concentrations for 15 hours or with 3mM propionate for the indicated times.

(a) The expression level of Phospho-Akt, PTEN and Class I/III PI3 Kinase were detected by Western blot.

(b) The phosphorylation status of AMPK α/β subunits and an AMPK downstream effector acetyl-coA carboxylase were detected by Western blot. The data represent as least three independent experiments.

(c) The expression level of AMPK α in the HCT116 cells which are infected with AMPK α in the presence or absence of doxycycline (Dox) was examined. The direct downstream target of mTOR pathway (p70S6) and several autophagy markers were examined by western blot.

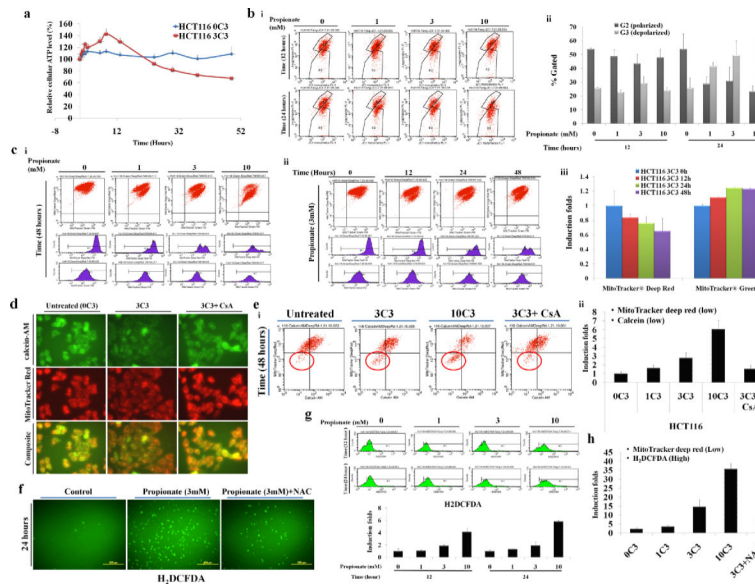


Figure 4. Propionate-induced AMPK signaling activation is associated with mitochondrial defect-induced cellular ATP depletion and oxidative stress

- (a) HCT116 cells were treated with propionate (3mM) for the indicated times. The intracellular ATP level was measured using a CellTiter-Glo® Luminescent Cell Viability Assay kit. The bars represent the mean \pm SE (n=4).
- (b) HCT116 cells were treated with propionate (0, 1, 3, 10 mM) for the indicated times and were stained against JC-1 for flow cytometry. There was a significant increase in the number of cells with lowered red fluorescence [FL-2 (R3)], indicating a change in the ψ (i). The percentage of cells with polarized versus depolarized ψ was presented as bar graph (ii). The bars represent the mean \pm SE (n=3).
- (c) Mitochondria were stained with MitoTracker Deep Red and MitoTracker Green FM simultaneously, and the staining intensities were determined by flow cytometry (i and ii), with the mean fluorescence presented in the bar graph (iii). The bars represent the mean \pm SE (n=3).
- (d) HCT116 cells were treated with propionate (3mM) in the absence or presence of cyclosporin A (CsA, 2 μ M) for 24 hours. Then the cells were stained with calcein-AM, CoCl₂ and MitoTracker® Red. Representative images were obtained by fluorescence microscopy. Magnification, X600.
- (e) Propionate treated cells were stained with MitoTracker Deep Red and calcein-AM. The dyes intensities were analyzed by flowcytometry (i) and were presented as bar graph (ii). The bars represent the mean \pm SE (n=3).
- (f) HCT116 cells were treated with propionate (3mM) in the presence or absence of N-acetylcysteine (NAC) (1mM) for 24 hours and the cells were stained with Carboxy-H₂DCFDA for reactive oxygen species (ROS) detection and representative images were obtained by fluorescence microscopy. Magnification, X100.
- (g) Carboxy-DCF fluorescence was analyzed by flowcytometry.
- (h) HCT116 cells were treated with propionate (0, 1, 3, 10 mM) for 48 hours. The cells were stained with Carboxy-H₂DCFDA and MitoTracker Deep Red. The fluorescence intensities were analyzed by flow cytometry. The percentage of cells with enhanced Carboxy-

H₂DCFDA and reduced MitoTracker Deep Red staining were presented as bar graph. The bars represent the mean \pm SE (n=3).

Author Manuscript

Author Manuscript

Author Manuscript

Author Manuscript

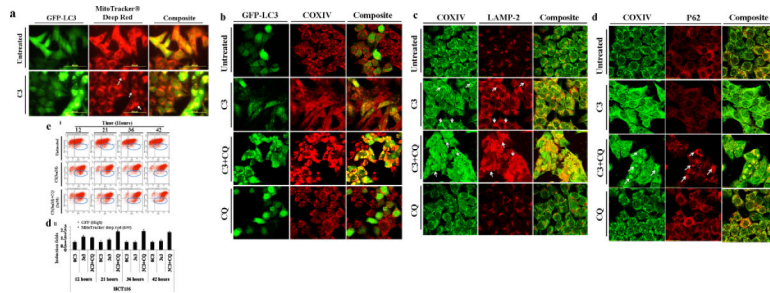


Figure 5. Defective mitochondria are targeted for autophagic degradation

(a) HCT116 cells with stable GFP-LC3 expression were treated with propionate (3mM) or vehicle control (PBS) for 24 hours. Mitochondria were stained by MitoTracker Deep Red, and representative images were obtained by fluorescence microscopy. Magnification, X600. Arrows indicate the cells with autophagy induction by propionate. Note the smeared mitochondria staining in the cells with autophagy activation, which is reflected by the formation of GFP-LC3 dots. Yellow in the merged image indicates colocalization of GFP-LC3 with mitochondria. The treated cells were also stained with COXIV antibody (b) for mitophagy detection with a confocal microscope.

HCT116 cells were treated with propionate (3mM) in the presence or absence of CQ (5uM) for 48 hours. The cells were stained with COXIV/LAMP2 (b) or COXIV/p62 (c) antibodies. Representative images were obtained with an Olympus Fluoview confocal microscope using a 60× oil immersion objective lens. HCT116 cells with stable GFP-LC3 expression were treated with propionate (3mM) in the presence or absence of CQ (5uM) for the indicated times. The GFP-LC3 and MitoTracker Deep Red fluorescence were analyzed by flow cytometry (ei) and the proportion of cells with increased GFP fluorescence and reduced MitoTracker Deep Red staining was presented as bar graph (eii). The bars represent the mean \pm SE (n=4). Arrows indicate the cells with autophagy induction by propionate.

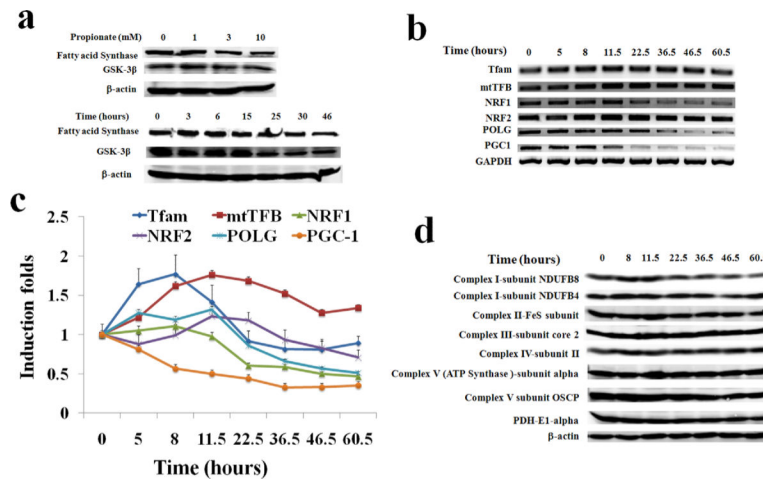


Figure 6. Rescue of cellular energy crisis through mitochondria biogenesis and alteration of glycogen and lipid metabolic pathways

(a) HCT116 cells were treated with propionate at different concentrations for 24 hours (top) or with 3mM propionate for the indicated times (bottom). The expression level of fatty acid synthase and GSK-3 β was determined by Western blot. The expression profile of genes regulating mitochondrial biogenesis in HCT116 cells after propionate treatment was evaluated by both semiquantitative reverse transcriptase PCR (RT-PCR) (b) and Real-time PCR (c). The bars represent the mean \pm SE (n=4). Nuclear gene mitochondrial transcription factor A (Tfam); mitochondrial transcription factor B (mtTFB); nuclear respiratory factors-1 and -2 (NRF-1 and -2); DNA polymerase gamma (Pol- γ); and peroxisome proliferator activated receptor co-activator 1 (PGC-1). (d) The protein level of mitochondrial redox carriers' subunits was examined by Western blot.

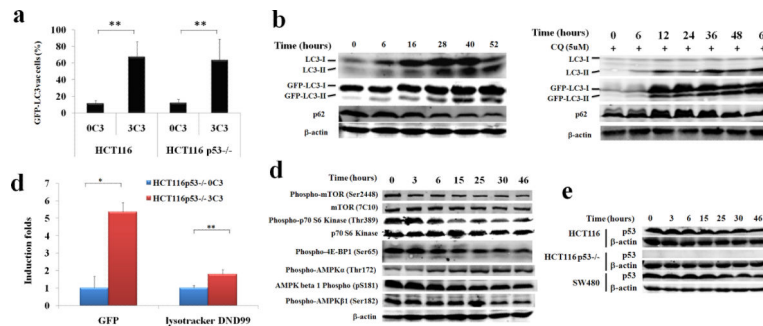


Figure 7. Propionate modulated autophagy induction and mTOR inhibition is independent of p53

- (a) HCT116 p53^{-/-} cells with stable GFP-LC3 expression were treated with propionate (3mM) for 36 hours. The percentage of cells with GFP-LC3 dots is represented as “GFP-LC3vac cells (%)”. A minimum of 100 GFP-LC3 expressing cells was counted. ** P<0.001, compared with PBS control at the corresponding time.
- (b) HCT116 p53^{-/-} cells with stable GFP-LC3 expression were subjected to propionate (3mM) in the absence or presence of Chloroquine (5uM) for the indicated times. The cell Lysates were immunoblotted against several autophagy markers.
- (c) Acidic vesicular organelle formation was evidenced by increased GFP fluorescence and elevated LysoTracker staining. *P <0.01; ** P<0.001, compared with PBS control at the corresponding time.
- (d) HCT116 p53^{-/-} cells were treated with propionate (3mM) for the indicated times. Western blot analysis was used to detect several markers regarding to mTOR pathway and AMPK pathway regulation.
- (e) The expression level of p53 was examined by Western blot in HCT116 and SW480 cells following propionate (3mM) treatment.

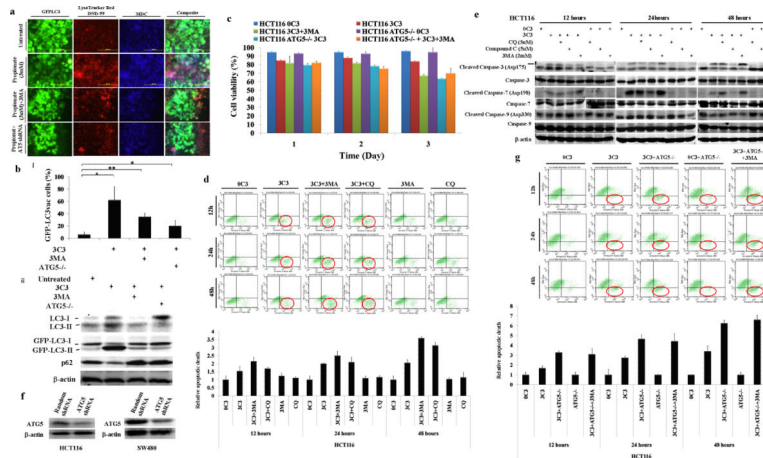


Figure 8. Inhibition of autophagy potentiates propionate-induced apoptotic cell death (a) HCT116 cells were treated with propionate (3mM) for 36 hours in the absence or presence of 3-MA (2mM). The same treatment was applied to the cells infected with *ATG5* shRNA. Acidic vesicular organelle formation was detected by LysoTracker Red DND-99 and MDC staining. Representative images are all taken at 600× magnification with a fluorescence microscope. (b) Punctate GFP-LC3 marked autophagosome formation was quantified (i). Data were presented as “GFP-LC3vac cells (%)” (bi). *, $P < 0.05$; **, $P < 0.001$, compared with a PBS control. Several autophagy markers were evaluated by western blot (ii). HCT116 cells pretreated with 3-MA (2mM) or infected with *ATG5* shRNA were subjected to propionate (3mM) for the indicated times. The cell viability was measured by trypan blue exclusion based cell staining (c), and the apoptotic cell death was evaluated by phosphatidylserine (PS) based annexin V staining (d, g). (e) Western blot analyses of caspase-7 and caspase-3 cleavage in HCT116 cells treated with propionate (3mM) for the indicated times in the absence or presence of autophagy inhibitors (3-MA and CQ) or AMPK inhibitor (Compound C). (f) HCT116 and SW480 cells were infected with *ATG5* shRNA, and the protein knockdown was evaluated by Western blot.

Table 1

ATG5 shRNA constructs	Sequences
TI358433	GTGCTTCGAGATGTGTGGTTGGACGAAT
TI358435	AAGCACTTTCAGAAGGTTATGAGACAAGA
TI358434	TCAGCTCTTCCTGGAAACATCACAGTACA
TI358436	GCAATCTTGTAACCTTGATAATGAACAGT

Author Manuscript

Author Manuscript

Author Manuscript

Author Manuscript

Table 2

RT-PCR primer sequences

Gene	Sequence 5'-3'	Size (bp)
Tfam	Sense CCACCGGAGCGATGGCGTTT Antisense CTGAAGGGGGAGCGCAGTCG	112
mtTFB	Sense CGTGGGCGTGGTGCCTCA Antisense CAGCCTGCCCGTCTTCCA	169
NRF1	Sense GCGCAGCCGCTCTGAGAACT Antisense CAGCAGCGGCCATTCCACA	269
NRF2	Sense GGCTGCTGCACTGGAAGGCT Antisense TCTCCCGAGGAACCCGCTG	216
POLG	Sense ACCGGAAGCACCGTGAGGA Antisense GCAGGCGGCTCATGGTTGGT	197
PGC1	Sense GCCGTGGCCGAGAAATGAC Antisense GCCTGTGGCATCCGCCAAA	578
hGADPH	Sense GGCCTCCAAGGAGTAAGACC Antisense AGGGGTCTACATGGCAACTG	147

Author Manuscript

Author Manuscript

Author Manuscript

Author Manuscript